Measurements of magnetic field fluctuations using an array of Hall detectors on the TEXTOR tokamak

I. Ďuran[a] and J. Stöckel
Institute of Plasma Physics, Association EURATOM/IPP.CR, Praha 182 21, Czech Republic

G. Mank, K. H. Finken, and G. Fuchs
Institut für Plasmaphysik, Association EURATOM-KFA, TEC partner, D-52425 Jülich, Germany

G. Van Oost
Department of Applied Physics, Ghent University, B-9000 Gent, Belgium

Hall detectors have been used to measure the magnetic field together with its' fluctuations in the boundary of a tokamak. The results show, that the measurements which have been performed so far, mainly by use of coils together with subsequent integration, either on-line or later by computer, can be substituted by Hall probe measurements giving the desired value of B directly. Because the integration of the coil signal becomes more and more difficult with long pulses, Hall detectors may give advantages in future fusion devices. We implemented a stack of nine Hall detectors mounted on three planes on a rod in such a way, that the three components of the magnetic field can be measured. To avoid capacitive and charge pickup from the plasma, the probes are electrically shielded. The damping due to skin effect within this shield has been taken into account. The probes have been calibrated using a known magnetic field of a straight wire driven with a LC bank. This field has been precisely measured with a Rogowski coil. The dependence of the Hall coefficient on the frequency has been measured and the pickup in the feeds due to $\dot{B}$ has been withdrawn from the results. We demonstrate the method with measurements on the TEXTOR tokamak, where we could clearly detect the small stray fields associated with magnetohydrodynamic (MHD) fluctuations. On TEXTOR we have been able to detect the MHD activity preceding discharge disruptions as well as the precursors of the so called sawteeth. The results are compared to those of other diagnostics on TEXTOR as, e.g., magnetic loops and electron cyclotron emission, and they do well compare. © 2002 American Institute of Physics. [DOI: 10.1063/1.1502018]

I. INTRODUCTION

The research on nuclear fusion is aimed to construct a reactor in which the isotopes D and T of hydrogen are fused to produce helium and energy in form of 14.1 MeV neutrons and 3.5 MeV alpha particles. The kinetic energy of the neutrons can be converted into heat and finally into electric power. To achieve this goal, temperatures in the order of 200 MK together with a density of several 10^{19} m^{-3} and a confinement time of several seconds are needed.

In stellarators and tokamaks[1] magnetic fields with a toroidal shell structure are used to achieve plasma confinement. The exact shape of these fields is essential to achieve the earlier goals. In the plasma interior magnetic fields can be measured with spectroscopic methods; these measurements are rather difficult. From measurements of the magnetic fields done outside the plasma many important properties like the plasma current, the energy content and magnetohydrodynamic (MHD) fluctuations together with their mode structure can be inferred.

Such measurements have in the past been done using different types of coils. As the time duration of the experiments has increased during the last years, the evaluation of the magnetic field B from the measured $\dot{B}$ has become more difficult, because the integration needs a precise determination of possible offsets in the preamplifiers, see, e.g., Refs. 2 and 3.

There are two advantages of Hall probes as compared to coils.

- There is no limit on the time duration, because they measure B directly.
- They can be smaller and measure mode structures of higher order.[4]

The major drawbacks are:

- They are not vacuum proof—at least not at elevated temperatures.
- The output voltage is low, therefore, any pickup of stray signals on both loops, the current feed and the output contacts can complicate the data interpretation.

The typical Hall detectors are operational up to temperatures around 100 °C. Because the tokamak chamber often reaches temperatures well above this limit, the Hall probe has to be cooled. To eliminate capacitive coupling with the plasma, the Hall detectors have to be shielded by a conductive shell. The damping rate of the magnetic field oscillations

FIG. 1. Principal scheme of Hall detectors for a N type semiconductor.
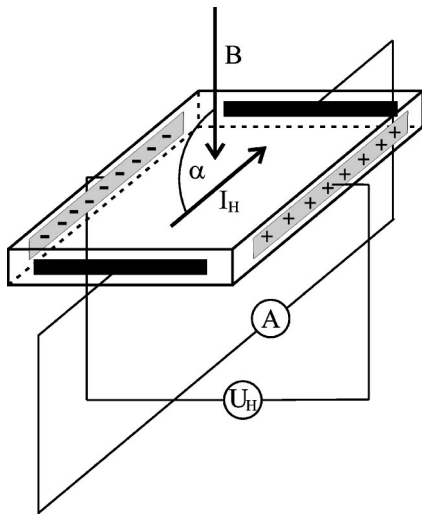

FIG. 2. Layout of the Hall detector.

penetrating this conductive shell has to be taken into account.

The structure of the article is as follows. The fundamentals of the Hall effect from the point of view of classical electrodynamics are briefly reviewed in Sec. II. Then, the Hall probe diagnostics used at TEXTOR is described in Sec. III A. Results and analysis of the absolute calibration are presented in Sec. III B. Several examples illustrating possible applications of the Hall probes in fusion devices are mentioned in Sec. IV. Finally, the article is summarized.

II. PHYSICAL PRINCIPLE OF HALL DETECTOR

The Hall effect was first observed in 1879 by Hall at the Johns Hopkins University. Take a slab of conductor or semiconductor material (see Fig. 1) and drive a constant current I_H along it, then immerse the slab into a magnetic field B that points along the slab normal. A voltage U_H appears between the remaining two faces of the slab. This, at the time of its discovery a very puzzling observation, is called Hall effect. Its' precise treatment is rather complicated and involves quantum mechanics.[5,6] Here it will be described from the viewpoint of classical electrodynamics only.[7] The current I_H driven through a N type semiconductor or conductor is carried by electrons. Electrons moving with velocity v are affected by the external magnetic field B and see a Lorentz force $F = q(E + v \times B)$. This force causes the electrons to drift toward one side of the Hall plate which establishes an electric potential U_H as depicted in Fig. 1. For P type semiconductors, the situation is similar, only the polarity of the Hall voltage U_H being reversed.

The voltage U_H is given by the following equation:

$$U_H = k_H I_H B \sin(\alpha),\tag{1}$$

where α is the angle between B and I_H and k_H is the Hall coefficient. k_H depends on the semiconductor material chosen, on the slab area facing B, and also on temperature. Note, that according to Eq. (1), the Hall element can also be used as analog multiplier for the quantities I_H and B. For measure-
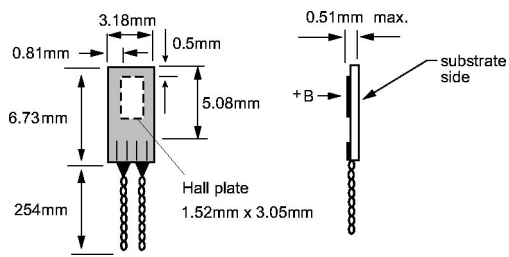
ment of the magnetic field, it is desirable to keep I_H and $\sin(\alpha)$ constant, therefore, it is possible to introduce a Hall constant k as $k = k_H I_H \sin(\alpha)$.

For oscillating magnetic fields, Eq. (1) should be rewritten in order to allow for a phase shift:

$$U_H(t,f) = k(f) B_{max} \sin[\omega t + \varphi_{Hall}(f)],\tag{2}$$

where $k(f)$ depends on frequency and $\varphi_{Hall}(f)$ is the phase shift caused by the finite time of response of the Hall detector to the applied magnetic field. The experimental determination of the $k(f)$ and $\varphi_{Hall}(f)$ functions is given in Sec. III B.

III. EXPERIMENTAL ARRANGEMENT

A. Diagnostics setup

A probe head, containing an array of nine air-cooled Hall detectors was constructed and used on TEXTOR to monitor all three components of the magnetic field inside the tokamak chamber. For this purpose, commercially available bulk Indium Arsenide Hall detectors F.W. Bell BH-705, with active area 1.52×3.05 mm and width 0.13 mm, have been used. Each Hall detector is mounted on a substrate plate having the dimensions $3.18 \times 6.73 \times 0.38$ mm (see Fig. 2).

According to the manufacturer, the sensitivity of each Hall detector is 0.1 V/T$\pm 25\%$ at 100 mA driving current I_H. For 0.1 mT this implies a rather low output voltage of $U \sim 10 \mu$V. Therefore, the Hall detector output signal has to be amplified, processed by analog filters, and finally digitized and stored for further numerical processing. The block diagram of the detection system used is schematically shown in Fig. 3.
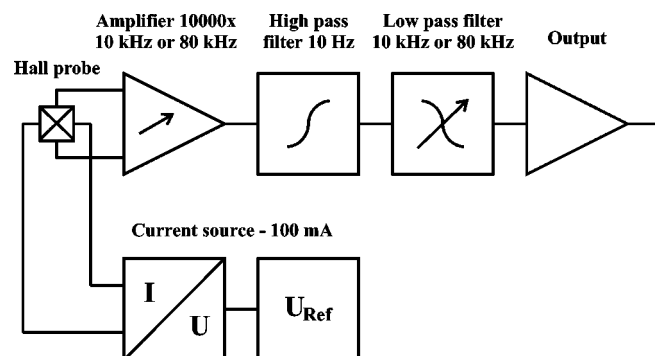

FIG. 3. Schematic diagram of the Hall probe detection system: current source, amplifier, and analog filters. In most of the experiments 10 kHz amplifiers and low pass filters have been used.
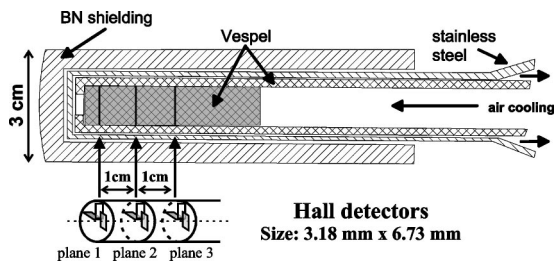
FIG. 4. Construction of the Hall probe.

The filtering serves the following purposes: to suppress (if desired) the direct current toroidal magnetic field and its' stray components due to not perfect alignment of the detectors. The low pass filters 10 or 80 kHz serve as antialiasing filters for the analog to digital converters whereby for the latter we did have only one channel.

In the range $-20-+80\,°C$, the sensitivity of the Hall detectors decreases linearly with temperature with mean coefficient $-0.08\%/°C$. In case of an ideal source for the driving current I_H, the temperature coefficient of the Hall detector resistivity can be neglected. Then, an increase of the Hall detector temperature by $\sim 12\,°C$ results in a 1% decrease in sensitivity of the diagnostics only. The operating temperature range of the Hall detectors is $-65-+100\,°C$ and the temperature must not exceed $105\,°C$. Therefore, the probe head is air cooled to avoid damage of the Hall detectors during heating of the tokamak chamber walls to several hundred degrees Celsius. The actual temperature inside the probe head is monitored by a temperature sensor.

As shown in Fig. 4 the Hall detectors are mounted in a slotted vespel support rod and they are inserted into a vacuum proof stainless steel tube with wall thickness of $d = 1\,mm$. This tube is the primary vacuum barrier separating the interior of the tokamak chamber from the air pumped into the probe head at a maximum pressure of 2 bar. This conductive housing is also necessary to minimize the electrostatic coupling with the plasma. The attenuation of the magnetic field oscillations due to the skin effect of this conductive housing is treated in more detail in Sec. III B. The probe head is further protected against excessive heat loads by a boron nitride cap.

The detectors are arranged in three measuring planes, spaced by 1 cm. On each measuring plane the three detectors are mounted perpendicular to each other such that, all three components of the magnetic field can be measured. As a result, it is possible to simultaneously measure B_r, B_θ, and B_T, and their fluctuations at three radial locations in a single

shot. The probe head is mounted on a movable holder and inserted into the tokamak chamber vertically from the top. The experiments have been performed in the scrape-off-layer about 4 cm outside the last closed flux surface, i.e., in the area where the magnetic field lines intersect the material limiter.

B. Calibration

Each Hall detector was absolutely calibrated in the frequency range 1.4–100 kHz using an RLC oscillating circuit. Discharging a capacitor battery C (0.06–78 μF) into an inductance L (1.7–160 μH) followed by a long straight wire creates a damped sinusoidally oscillating current I_C with amplitude of tens of Ampèr within a time interval of several milliseconds. This current is measured by an absolutely calibrated Rogowski coil. According to Ampère's law, the current flowing through a long straight conductor induces an axial magnetic field with amplitude $B = \mu_0 I/2\pi r$ (several millitesla in this case) which is in the range of the oscillations[8] to be detected on TEXTOR. Placing a correctly oriented Hall probe at a known distance r from this long straight wire provides a method to absolutely calibrate the probe. The calibration frequency is varied by changing the circuit parameters C and L.

Neglecting damping, the calibration magnetic field B just outside the probe head is $B = B_{max}\sin(\omega t)$. The digitized output voltage from the single Hall detector was found as $U = U_{max}\sin[\omega t + \varphi(f)]$. The calibration constant for amplitude $K(f)$ was computed as

$$K(f) = U_{max}/B_{max}. \tag{3}$$

The phase shift calibration function $\varphi(f)$ has been computed using the formula

$$\cos(\varphi) = \frac{\langle U \cdot B \rangle}{\sqrt{\langle U^2 \rangle \cdot \langle B^2 \rangle}}, \tag{4}$$

where $\langle \rangle$ denotes the time average.

The diagnostic was absolutely calibrated in the two setups of the electronics, one with amplifiers with the 10 kHz frequency limit and the second with 80 kHz limit (see Fig. 3).

1. Calibration—10 kHz setup

In this section, results of the calibration of the three radial Hall detectors including the amplifiers are presented. The amplitude $K(f)$ and phase shift $\varphi(f)$ calibration functions are shown in Fig. 5.
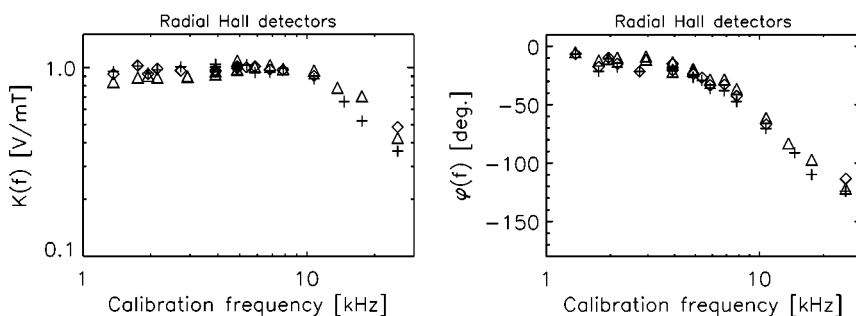

FIG. 5. Calibration curves of radial Hall detectors in the 10 kHz electronics setup. Left panel: calibration constant $K(f)$. Right panel: phase shift calibration $\varphi(f)$. Each of the three marks (triangle, cross, and diamond) corresponds to a single radial Hall detector.
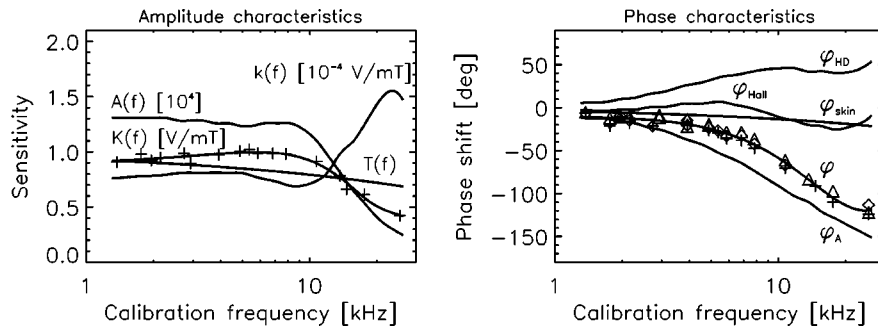
FIG. 6. Left panel—measured transmission functions of the whole diagnostics $K(f)$, the amplifier, the filters $A(f)$, the computed attenuation factor due to the skin effect of the probe's conductive housing $T(f)$, and the sensitivity of the Hall detector relating to the Hall effect only $k(f)$. Right panel—measured phase shifts caused by the amplifier and the filters φ_A and the overall phase shift of the diagnostics φ, and the computed phase shifts caused by the skin effect of the probe's conductive housing φ_{skin}, by the Hall effect itself φ_{Hall}, and by the mixing of the Hall and the inductive component of the voltage generated by the Hall detector φ_{HD}.

It is seen from the left panel that the calibration constant $K(f)$ is almost independent of the frequency in the range 1–10 kHz with a value of ~1 V/mT for all the three radial Hall detectors. The right panel shows the variation of the overall phase shift $\varphi(f)$ of the diagnostics. It is linearly increasing with frequency from 0° up to 90° in the range 1–15 kHz.

In order to understand these results, it is necessary to discuss the physical mechanism acting in the Hall probe detection system in more detail. Four processes affect the probe's amplitude and phase characteristics.

(1) The Hall effect itself as described in Sec. II;
(2) the inductive pickup of the magnetic field in the small loops present in the measuring circuit especially in the connectors of the Hall detector;
(3) the skin effect of the probe's conductive housing; and
(4) the nonideal transmission functions of the amplifiers.

Consequently, the calibration constant $K(f)$ has contributions from other voltages that are due to the amplifier characteristics $A(f)$, skin effect $T(f)$ and pickup in the feeds for the driving current[9] and mainly in the feeds for the detection $I(f)$:

$$K(f) = A(f)T(f)I(f). \tag{5}$$

The dimensionless factors $A(f)$ and $T(f)$ describe respectively the amplification and the attenuation of the signal. The function $I(f)$ given in volts per tesla says how much voltage is generated in the Hall detector via Hall effect and inductive pickup. The phase shift has contributions from the same sources:

$$\varphi(f) = \varphi_A(f) + \varphi_{\text{skin}}(f) + \varphi_{\text{HD}}(f). \tag{6}$$

When the quantities except for $I(f)$ and $\varphi_{\text{HD}}(f)$ are known from extra measurements these two missing can be calculated (cf. Fig. 6). Let us discuss these phenomena in more detail.

a. Amplifier and filters. The transfer function of the amplifier and filters is easily measured by replacing the Hall detector by a calibrated wave generator.

b. Skin effect. As outlined earlier, the Hall detectors are mounted in a stainless steel casing with wall thickness d

$=1$ mm. We calculate the reduction and phase shift, which is experienced by the magnetic field using the formula

$$B_{\text{in}} = B_{\text{max}} e^{-s(f)d} \sin[\omega t - s(f)d]$$
$$= B_{\text{max}} T(f) \sin[\omega t + \varphi_{\text{skin}}(f)], \tag{7}$$

whereby $s(f) = \sqrt{\omega\mu\sigma/2}$, and we used relative permeability $\mu_r = 1.02$ and conductivity $\sigma = 1.33 \, 10^6 \, \Omega^{-1} \, \text{m}^{-1}$.

c. Inductive pickup. An additional effect, which gives rise to errors is the induction of a voltage in small loops formed by the Hall detector's connectors. This voltage U_{ind} is proportional to the total effective area of the loop S and to the time derivative of the magnetic field crossing this loop, hence $U_{\text{ind}} = S dB/dt$. Assuming an harmonic evolution of B as $B_{\text{max}} \sin(\omega t)$, then $U_{\text{ind}} = 2\pi f S B_{\text{max}} \cos(\omega t)$. As the Hall voltage is typically low, i.e., ~10 μV for 0.1 mT, already a small loop ~1 mm^2 is sufficient to induce a comparable voltage at frequencies above 10 kHz. Note also that for a given S, the induced voltage U_{ind} increases linearly with the frequency of the magnetic field. The value of S for the used Hall detectors was supplied by the manufacturer. When the Hall detector is put into a known oscillating magnetic field and the driving current I_H is switched off, the output voltage is proportional only to the inductive part so that S can be determined.

d. Derivation of the Hall effect characteristics $k(f)$ and $\varphi_{\text{Hall}}(f)$ from the calibration measurements. In the following, a procedure to obtain $k(f)$ and $\varphi_{\text{Hall}}(f)$ from the measured quantities is presented. The amplitude $k(f)$ and the phase characteristics $\varphi_{\text{Hall}}(f)$ of the Hall effect are difficult to measure separately; this is, because there is an inductive component which is intrinsically present in the Hall detector signal.

Supposing that the conductors to the amplifier are correctly twisted and neglecting electrostatic pickup, the total voltage at the input of amplifier U_{HD} is the sum of the Hall and inductive voltages

$$U_{\text{HD}} = U_{\text{Hall}} + U_{\text{ind}}. \tag{8}$$

For simplicity, in the following the dependence on frequency is not explicitly stated, whereas this dependence is
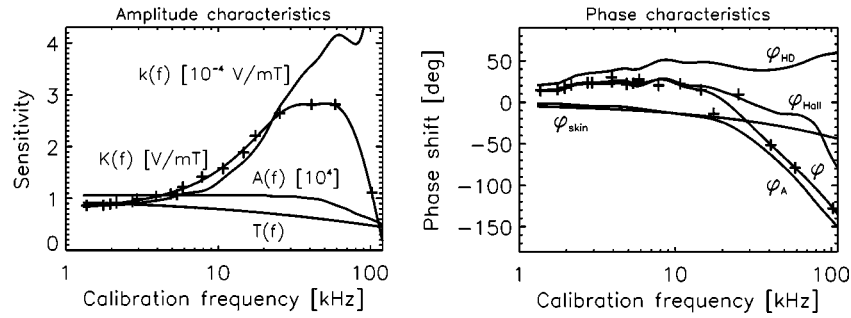
FIG. 7. Left—measured transmission functions of the whole diagnostics $K(f)$, the amplifier, the filters $A(f)$, the computed attenuation factor due to the skin effect $T(f)$ and the sensitivity of the Hall detector corresponding to the Hall effect $k(f)$. Right—measured phase shifts caused by the amplifier and the filters φ_Λ and the overall phase shift of the diagnostics φ, and the computed phase shifts caused by the skin effect of the probe's conductive housing φ_{skin}, by the Hall effect itself φ_{Hall}, and by the mixing of the Hall and the inductive component of the voltage generated by the Hall detector φ_{HD}.

maintained in the text. Substituting for U_{HD}, U_{Hall}, and U_{ind} and taking the skin effect into account Eq. (8) becomes

$$ITB_{\max} \sin(\omega t + \varphi_{\text{skin}} + \varphi_{\text{HD}}) = TkB_{\max} \sin(\omega t + \varphi_{\text{skin}}$$
$$+ \varphi_{\text{Hall}}) + 2\pi f STB_{\max} \cos(\omega t + \varphi_{\text{skin}}), \quad (9)$$

where $k(f)$ is the sensitivity of Hall detector corresponding to the Hall effect and $S = 1.35\ \text{mm}^2$ is the inductive area of the Hall detector and its connector. The value of $\varphi_{\text{HD}}(f)$ depends on $\varphi_{\text{Hall}}(f)$ and on the ratio of amplitudes in front of the sine and cosine on the right-hand side of Eq. (9), i.e., on the ratio of the Hall and the inductive part of the signal. After rewriting Eq. (9) one obtains

$$I \cos(\varphi_{\text{HD}}) \sin(\omega t + \varphi_{\text{skin}}) + I \sin(\varphi_{\text{HD}}) \cos(\omega t + \varphi_{\text{skin}})$$
$$= k \cos(\varphi_{\text{Hall}}) \sin(\omega t + \varphi_{\text{skin}}) + [k \sin(\varphi_{\text{Hall}})$$
$$+ 2\pi f S] \cos(\omega t + \varphi_{\text{skin}}). \quad (10)$$

Comparing the amplitudes in front of the terms $\sin[\omega t + \varphi_{\text{skin}}(f)]$ and $\cos[\omega t + \varphi_{\text{skin}}(f)]$ on both sides of Eq. (10) one obtains a system of two equations for two unknown functions $k(f)$ and $\varphi_{\text{Hall}}(f)$:

$$I \sin(\varphi_{\text{HD}}) = k \sin(\varphi_{\text{Hall}}) + 2\pi f S, \quad (11)$$

$$I \cos(\varphi_{\text{HD}}) = k \cos(\varphi_{\text{Hal}}). \quad (12)$$

An expression for $\varphi_{\text{Hall}}(f)$ is obtained dividing Eqs. (11) and (12):

$$tg(\varphi_{\text{Hall}}) = \frac{I \sin(\varphi_{\text{HD}}) - 2\pi f S}{I \cos(\varphi_{\text{HD}})}. \quad (13)$$

Then, the Hall constant $k(f)$ can be obtained using any of the Eqs. (11) and (12).

The frequency dependence of k, K, A, T (left) and the phase shift characteristics (right) are shown in Fig. 6.

It is seen that value of $k(f)$ is almost constant in the frequency range 1.4–10 kHz and its value $\sim 0.75\ 10^{-4}$ V/mT corresponds to the value provided by the manufacturer for a stationary magnetic field 10^{-4} V/mT $\pm 25\%$. For frequencies above 10 kHz it is rapidly increasing. The phase shift $\varphi_{\text{Hall}}(f)$ of the signal caused by the Hall effect is about zero $\pm 20°$. Considering the inaccuracies and uncertainties of the calibration measurement, this tells that the Hall detector responds in this frequency range immedi-

ately to the magnetic field. Therefore, the phase shift induced in the Hall detector $\varphi_{\text{HD}}(f)$ is only due to mixing of the Hall and the inductive parts of the signal. The attenuation factor due to the skin effect $T(f)$ of the probe's 1-mm-thick stainless steel conductive housing ($\mu_r = 1.02$, $\sigma = 1.33\ 10^6\ \Omega^{-1}\ \text{m}^{-1}$) reaches $\sim 80\%$ and starts to become significant at the frequency 10 kHz.

2. Calibration—80 kHz setup

One of the radial Hall detectors has in addition been calibrated in the experimental setup with the 80 kHz amplifier and the low pass filter (see Fig. 3). The same calibration measurement and analysis was used as described in the previous section. It is necessary to stress that only a few calibration measurements were done for frequencies above 10 kHz in this setup. Because of low statistics, results presented in this section are only qualitative. The frequency dependence of the resulting amplitude (left) and the phase (right) characteristics are shown in Fig. 7.

The $k(f)$ and $\varphi_{\text{Hall}}(f)$ curves shown in Figs. 6 and 7 give in the frequency range 1–30 kHz the expected results, because they are properties of the Hall detector and should not depend on the amplifier and filters used. The difference is caused by small frequency resolution for frequencies above 10 kHz and also by the inaccuracy of the calibration measurements. The $k(f)$ keeps increasing up to 100 kHz. Note the attenuation of the magnetic field due to the skin effect seen from the decrease in the $T(f)$ curve. The amplitude of the measured magnetic field is reduced by the probe's conductive shell to one half at 100 kHz. A more detailed study of the theory of the Hall effect is required to learn more about the observed shape of $k(f)$.

3. Summary of calibration measurements

The results of calibration measurements and analysis may be summarized as follows.

- It has been shown that a diagnostics based on Hall detectors does allow measurements of magnetic fluctuations <0.1 mT within the frequency range 1–100 kHz and with sufficient sensitivity.

- Careful avoiding of any inductive loops (as small as 1 mm^2) in the measuring circuit is critical for the mea-
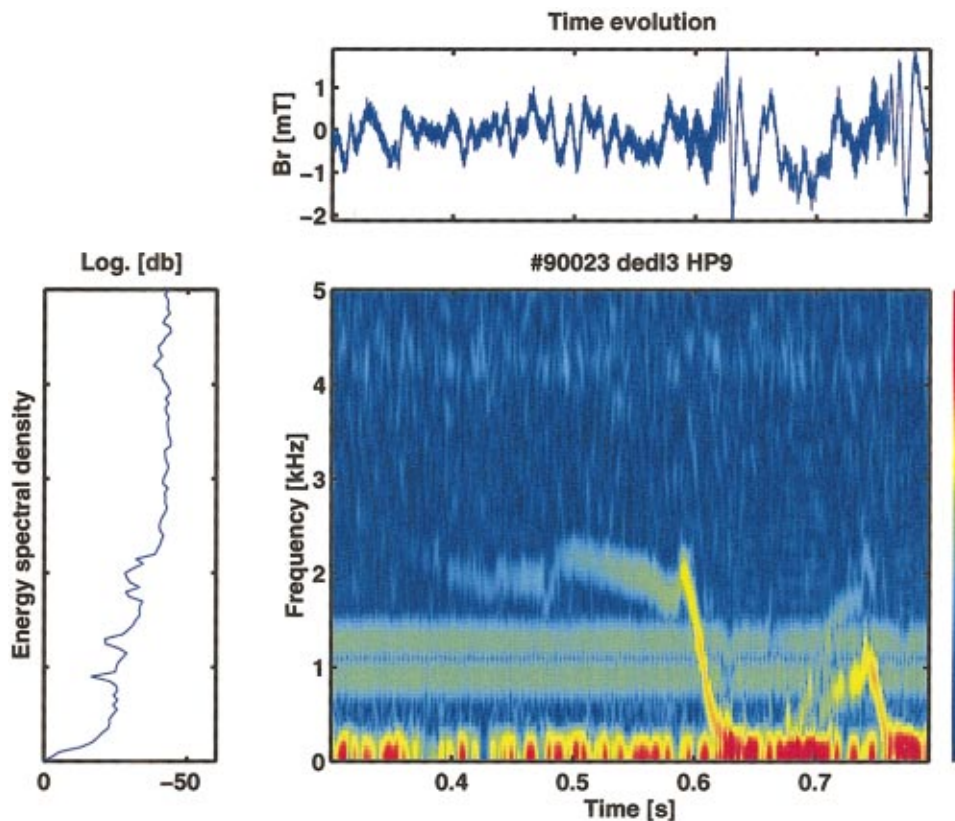
FIG. 8. (Color) Time-frequency plot of B_r signal during disruption (central panel). The top panel shows the time trace of the measured B_r signal. The left panel displays the energy spectral density integrated over the entire time of the time-frequency plot.

surements of the magnetic field oscillations in the kilohertz range of frequencies. If such loops cannot be avoided completely, one may think of compensating them by artificial ones.

- The skin effect of the probe's conductive housing plays an important role for frequencies above ~10 kHz. Improved technical solutions of the probe head allowing proper cutting of the conductive housing would be highly desirable if to operate in the 100 kHz range.

- The response time of the Hall detector to the measured magnetic field via Hall effect given by $\varphi_{Hall}(f)$ was found to be immediate in the frequency range 1–60 kHz.

- The Hall constant $k(f)$ is constant for frequencies 1–10 kHz and increases for higher frequencies. This observation should be compared with a detailed theoretical treatment of the Hall effect.

- Calibration errors are mainly caused when the probe is not precisely aligned perpendicular to the measured magnetic field. Improvements of the calibration method are under investigation.

IV. EXAMPLES OF EXPERIMENTAL RESULTS OBTAINED USING THE HALL PROBE

The measurements and the data evaluation given in this section have been obtained for a variety of experimental regimes on TEXTOR and they are primarily intended to demonstrate the capability of the Hall probes for field and fluctuation measurements in tokamak plasmas; it is not our ambition to go too deeply into each subject (see, e.g., Refs. 10–14 for more detailed studies on the subjects discussed later).

A. Study of disruptions

Several experimental campaigns on TEXTOR have been dedicated to the study of disruptions.[11,12] During these discharges a pronounced MHD activity shows up, which makes these discharges a good testbed for magnetic diagnostics.

Figure 8 shows in its' upper panel a time trace of the Hall probe signal measuring the radial magnetic field component during the last 0.5 s of discharge No. 90023 which terminated due to a disruption. The onset of a MHD activity is apparent at 0.63 s and a major disruption follows at 0.79 s. The left panel of Fig. 8 shows the spectral density of the signal mentioned earlier. The two-dimensional plot in the middle is a time-frequency (TF) representation of the measured signal computed using the windowed Fourier transform. Two features dominate the plot. The magnetic feedback positioning system of TEXTOR causes, over the entire discharge, a constant perturbation at the two fixed frequencies 0.9 and 1.3 kHz. An increase of the magnetic signal in the frequency band around 2 kHz is observed beginning at 0.4 s and it is caused by a growth of a MHD instability. In the time interval 0.6–0.63 s the frequency of MHD instability decreases below 300 Hz. This is accompanied by an increase of the amplitude B_r, which demonstrates a rapidly growing instability. After this first disruptive event the plasma recovers. However, the next MHD instability starting at 0.7 s leads to a major disruption.

The Hall probe signal corresponds well to those of the Mirnov coils measuring $\dot{B}_\theta$ (cf. Fig. 9) and to a local measurement of the electron temperature at the MHD mode position deduced from electron cyclotron emission at 105 GHz (cf. Fig. 9).
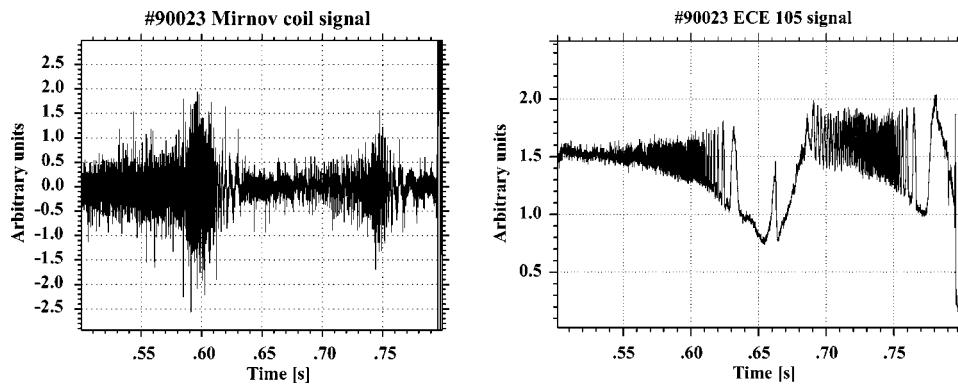
FIG. 9. Left panel—time trace of the signal measured by one of the Mirnov coils proportional to $\dot{B}_\theta$. Right panel—electron cyclotron emission signal proportional to the local value of temperature within the plasma region where MHD perturbation occurs.

B. Sawtooth precursors

The sawtooth crash in a tokamak is preceded by a $m = 1$ mode activity called precursors.[1,10] The recording of several sawteeth precursors is displayed in Fig. 10. The central TF plot is supplemented by a time evolution of the measured signal (upper plot) and the spectral density (left plot) as in Fig. 8.

The duration of a single sawtooth precursor can be as long as 20 ms. Shortly before (5 ms) the sawtooth crash we observe a jump of the oscillation frequency. The finding for this kind of discharge is somewhat outstanding, because in other ones we find a continuous change. Sawtoothing is not yet understood in all details.

C. Measurements during RI mode

The RI mode on TEXTOR is an experimental regime where improved confinement is obtained by edge cooling using noble gases, e.g., neon.[13,14] This edge cooling reduces turbulence preferentially in the high frequency band. We can confirm this as it becomes evident from Fig. 11. The top panel shows the time evolution of the B_r signal just before neon injection, while the middle panel shows that during RI mode. The bottom panel compares the frequency spectra corresponding to these two time intervals. A decrease of magnetic turbulence in RI mode over the whole spectrum is evident. However, we found this result only, when the ratio between outward thermal pressure and inward magnetic pressure called β_N had been feedback stabilized, whereas without stabilization the spectra looked similar, or even an increase of the turbulence was observed after neon injection.

Another feature of the magnetic turbulence during the RI mode is, that depending on the energy confinement time, the spectra show changes in the frequency band between 5 and 10 kHz, whereby the frequency of the dominant magnetic instability increases with confinement time. More measure-
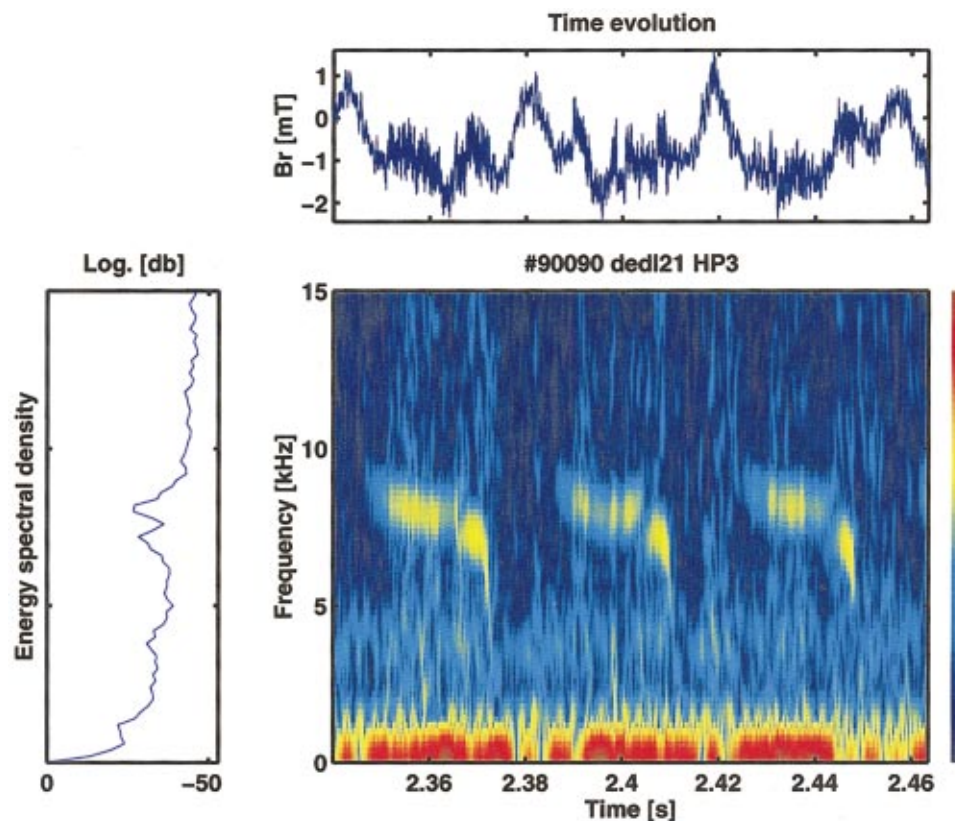

FIG. 10. (Color) Time-frequency record of sawteeth precursors (central panel). The top panel shows the time trace of the measured B_r signal. The left panel displays the energy spectral density integrated over the entire time of the time-frequency plot.
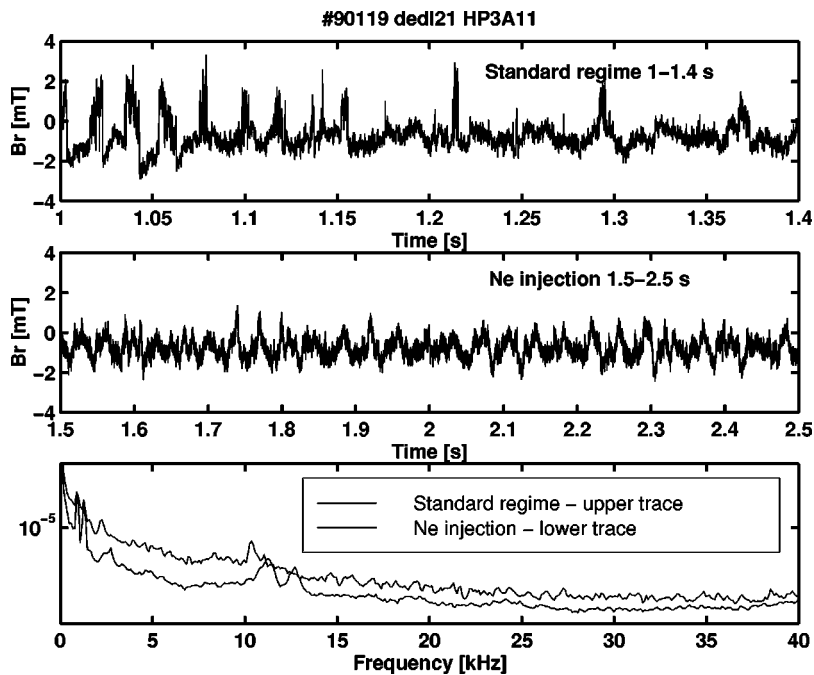
FIG. 11. Suppression of magnetic turbulence over the whole spectrum in RI mode with energy feedback.

ments and comparison of different profiles will be necessary in order to understand this finding.

V. CONCLUSIONS

An array of nine Hall probes has been successfully tested on the TEXTOR tokamak. The major advantage of Hall probes as compared to conventional magnetic coils is their smaller size and the direct relation of the measured signal to the magnetic field while maintaining a comparable sensitivity. Because Hall detectors are made of semiconductors, cooling is necessary. Sensitivity to high neutron fluxes has to be tested. The use of Hall probes for measurements of magnetic field oscillations above 100 kHz is limited by the inductive pickup by the Hall probe connectors, and depending on experimental setup also by the skin effect of the probes conductive shield. The results obtained during our experiments on TEXTOR illustrate the capability of Hall probes and they can be summarized as follows.

Magnetic instabilities have been detected and the time evolution of their rotation frequency could be followed. Sawteeth precursors together with their fine structure could be observed. An overall decrease of magnetic turbulence in RI mode discharges with energy feedback stabilization is ob-

served. There is a strong suspicion that, some features of the magnetic fluctuations frequency spectra measured during RI mode are directly related to plasma confinement, although the underlying physics is not understood yet. To refine the Hall probe diagnostics, more detailed studies are envisaged on TEXTOR as well as on the smaller tokamak CASTOR.

[1] J. Wesson, *Tokamaks*, 2nd ed. (Clarendon, Oxford, 1997).
[2] G. Fuchs, A. Krämer-Flecken, H. Larue, and W. Schalt, Fusion Eng. Des. **56–57**, 711 (2001).
[3] ITER physics expert group on diagnostics *et al.*, Nucl. Fusion **39**, 2541 (1999).
[4] The Mirnov coils on TEXTOR are made of Mo wire embedded in ceramic $2.5 \times 5 \times 10$ cm^3.
[5] E. H. Putley, *The Hall Effect and Related Phenomena* (Butterworths, London, 1960).
[6] A. C. Beer, *Galvanomagnetic Effects in Semiconductors* (Academic, New York, 1963).
[7] B. Drafts, Sensors 72 (1997).
[8] Of order per mile of the total field.
[9] This effect should be small.
[10] H. R. Koslowski *et al.*, Nucl. Fusion **40**, 821 (2000).
[11] K. H. Finken, A. Krämer-Flecken, G. Mank, and S. S. Abdullaev, J. Nucl. Mater. **290–293**, 1064 (2001).
[12] K. H. Finken, T. Denner, and G. Mank, Nucl. Fusion **40**, 339 (2000).
[13] A. M. Messiaen *et al.*, Phys. Plasmas **4**, 1690 (1997).
[14] G. Mank, Phys. Rev. Lett. **85**, 2312 (2000).